Nanoporous Materials

DOI: 10.1002/anie.201105190

Synthesis of Prussian Blue Nanoparticles with a Hollow Interior by Controlled Chemical Etching

*Ming Hu, Shuhei Furukawa, Ryo Ohtani, Hiroaki Sukegawa, Yoshihiro Nemoto, Julien Reboul, Susumu Kitagawa, and Yusuke Yamauchi**

Hollow particles, an important class of materials with large internal cavities and thin shells, present a wide range of potential applications,[1] such as energy storage,[2] chemical catalysis,[3] photonics,[4] and biomedical carriers.[5] The properties of hollow particles are strongly affected by the compositions and exquisite nanostructures of the shell regions. Many efforts have been made to control these parameters.[6,7] Recently, hollow particles with nanoporous shells have attracted great interest because the large pore volumes and high surface areas provided by the nanoporous shells show large storage capacity and allow guest species to pass easily into the internal cavity.[8–11] For instance, metal oxide hollow particles present a superior lithium storage capacity and good cycle performance,[2a,8] which could improve gas sensitivity[9] and catalytic performance[3a,10] in other applications.

Inspired by the superiority of nanoporous shells, the creation of microporous crystal shells with outstanding properties is also expected. Porous coordination polymers (PCPs) (or metal–organic frameworks, MOFs)[12] and zeolites are representative microporous crystals.[13] Having adjustable porosity and properties, microporous crystals show great potential in applications such as separation, catalysis, adsorption, and gas storage.[12,13] To date, however, there have been no reports on the successful synthesis of uniformly nanosized hollow particles with microporous crystalline shells.[14,15] Very few reports on microporous zeolite and PCP hollow particles have been published, and several problems have been encountered. A major problem is that the synthesized hollow particles are very large and have a broad size distribution.[14] Considering their practical use in various catalysis reaction processes, uniformly sized hollow particles are ideal because they can densely fill reactors or columns. Another problem is that the microporous crystallinity in the shells decreases seriously during the formation process (that is, amorphous regions are formed in the shells),[14e–g,15] causing a loss of thermal stability, acidic sites, and surface area. Therefore, the development of a general method of synthesizing uniformly nanosized hollow particles with highly crystalline microporous shells is in demand.

Herein, we present a facile route to the fabrication of uniform-sized Prussian blue (PB) hollow particles by utilizing a controlled self-etching reaction in the presence of PVP. PB crystals consisting of metal ions coordinated by CN bridges are very typical coordination polymers with a high surface area, showing excellent properties in many applications such as catalysis, sensors, molecular magnets, gas storage, and bioimaging.[16] The critical point in our procedure is the selection of PB mesocrystals as a starting material. PB mesocrystals are formed by the aggregation of PB nanocrystals in an oriented way, thereby showing single-crystal-like behavior.[17,18] Through small pores (or defects) in the aggregated PB nanocrystals, the etching solution can be diffused into the core of the mesocrystals. We succeeded in the formation of an interior hollow cavity with the retention of the original PB crystallinity. Although a few attempts to prepare PB hollow structures have been reported, the obtained shells were amorphous or poorly crystalline, with large organic impurities.[14e–g] Such hollow particles cannot show high surface areas and good magnetic responses.

Two types of PB mesocrystals with different particle sizes were used as starting materials (details regarding the synthetic conditions are given in the Experimental Section). SEM images indicated that the particle-size distributions of the original PB mesocrystals were very narrow and their average diameters were around 110 nm (Figure 1a) and 190 nm (Supporting Information, Figure S1a). From highly magnified SEM images (insets of Figure 1a; Supporting Information, Figure S1a), very rough surfaces were observed at the edges and corners of the cubes, suggesting that the cube shapes were created by the aggregation of small PB nano-

[*] Dr. M. Hu, Dr. Y. Nemoto, Prof. Dr. Y. Yamauchi
World Premier International (WPI) Research Center for Materials Nanoarchitectonics (MANA)
National Institute for Materials Science (NIMS)
1-1 Namiki, Tsukuba, Ibaraki 305-0044 (Japan)
E-mail: yamauchi.yusuke@nims.go.jp
Prof. Dr. S. Furukawa, Dr. J. Reboul, Prof. Dr. S. Kitagawa
Institute for Integrated Cell-Material Sciences (iCeMS)
Kyoto University, Yoshida, Sakyo, Kyoto 606-8501 (Japan)
and
ERATO Kitagawa Integrated Pores Project
(Japan) Science and Technology Agency (JST)
Kyoto Research Park, Bldg #3, Shimogyo, Kyoto 600-8815 (Japan)
R. Ohtani, Prof. Dr. S. Kitagawa
Graduate School of Engineering, Kyoto University
Katsura, Nishikyo, Kyoto 615-8510 (Japan)
Dr. H. Sukegawa
Spintronics Group, Magnetic Materials Unit
National Institute for Materials Science (NIMS)
1-2-1 Sengen, Tsukuba, Ibaraki 305-0047 (Japan)
Prof. Dr. Y. Yamauchi
Faculty of Science and Engineering, Waseda University
3-4-1 Ohkubo, Shinjuku, Tokyo 169-8555 (Japan)
and
Precursory Research for Embryonic Science and Technology
(PRESTO) (Japan) Science and Technology Agency (JST)
4-1-8 Honcho, Kawaguchi, Saitama 332-0012 (Japan)

Supporting information for this article is available on the WWW under http://dx.doi.org/10.1002/anie.201105190.

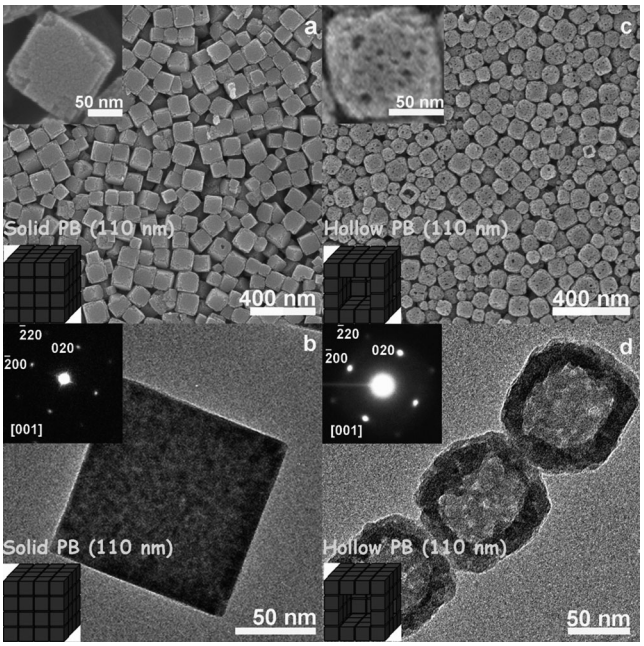

Figure 1. a) SEM and b) TEM images of solid PB mesocrystals (average particle size: 110 nm) as the starting material. c) SEM and d) TEM images of the hollow PB mesocrystals (average particle size: 110 nm) synthesized by chemical etching. Inset images on the SEM and TEM images are a), c) enlarged SEM images of one particle and b), d) the corresponding selected-area electron diffraction (ED) patterns of one particle.

particles.[17,18] Electron diffractions taken from one whole particle displayed very intense spots showing a single-crystal-like nature (Figure 1b; S1b), indicating the oriented aggregation of small PB nanocrystals. From a high-resolution image (Figure S2) of PB mesocrystals formed at a very early stage of growth (30 min), it was clarified that the cubic-shaped PB mesocrystals were formed by the oriented aggregation of small nanocrystals. Small pores (or defects) among the aggregated PB nanocrystals were also clearly observed (as indicated by the arrows in Figure S2).

To create an interior hollow cavity, the PB mesocrystals were treated with 1.0 M HCl solution at 140 °C for 4 h in the presence of PVP (details of the etching conditions are given in the Experimental Section). After the etching process, the average particle sizes were not significantly changed. Compared to that on the original PB mesocrystals, the surface on the particles became bumpy (Figure 1c; S1c). From TEM images, we confirmed that each of the resultant samples possessed a cube-shaped interior hollow cavity. The average sizes of the cavities were about 80 nm (Figure 1d) and 130 nm (Figure S1d). Surprisingly, intense diffractions were well preserved even after the formation of interior hollows. The phase purity of the samples was also examined by wide-angle XRD measurement (Figure S3). All the samples showed exactly the same diffraction patterns ($Fm\bar{3}m$) compared to the PB crystals (JCPDS card 73-0687). Our controlled etching process created an interior hollow cavity without changing the average particle size and without collapsing the original PB crystal structure.

It is well-known that crystalline PBs show a high surface area after the removal of water molecules.[16e,19] After degassing was performed under vacuum conditions at 40 °C for 60 h, N_2 adsorption–desorption isotherms were measured (Figure S4). The BET surface areas were drastically increased by the introduction of an interior hollow cavity. Steep increases at very low relative pressure were observed for all the samples before and after the etching, indicating the presence of micropores derived from PB crystals. After the etching, the adsorbed volumes in the adsorption isotherm gradually increased in the range of $P/P_0 = 0.5$–0.9, indicating the formation of mesopores with different sizes. The mesopores were observed in the PB shell regions in TEM images (Figure 1d; S1d). The appearance of hysteresis loops was caused by the presence of cage-type mesopores randomly connected with small windows. SEM and TEM observations and N_2 adsorption–desorption isotherms verified the realization of a hierarchically porous system consisting of three kinds of pores: 1) macropores (80 nm or 130 nm) derived from the interior hollow cavity; 2) mesopores (from 3.0 nm to 15 nm) formed in the shell regions; and 3) micropores (less than 1 nm) originating from PB crystals.

To investigate the formation mechanism in detail, we had to identify how the original PB mesocrystals were etched by the HCl solution. Time-dependent TEM images are shown in Figure S5. After 3.5 h, a very small interior cavity was formed in the center of the PB mesocrystals (Figure S5b). The cavity became larger after 4.0 h (Figure S5c), and all of the particles were destroyed after 4.5 h (Figure S5d). After over 5.0 h of etching, all of the PB nanoparticles were totally dissolved.

In the general etching process, the etching reaction normally starts from the external surface of the particles.[20,21] As a comparative experiment, when the PB single crystals (not the PB mesocrystals) were etched under the same conditions, the cubic-shaped single crystals were not converted to hollow particles, as confirmed by SEM imaging (Figure S6). In this case, the etching reaction started on the surfaces of single crystals, which led to the formation of large voids/holes (Figure S6b). The PB single crystals consisted of very compact, defect-free microstructures formed by an atom-to-atom crystallization process.[17] Therefore, HCl molecules as etching agents could not enter easily, which inhibited the formation of an interior hollow cavity. On the other hand, the PB mesocrystals used in this study had defects/voids (indicated by white arrows in Figure S2). Thus, it was possible for etching agents to diffuse into the inner parts of mesocrystals through the defects, leading to the formation of an interior hollow cavity.[6g,22]

The concentration of PVP is also an important factor in the appropriate surface protection of PB mesocrystals. When no PVP was dissolved, reproducibility was quite low, although a few particles possessed poorly defined hollow cavities (Figure S7a). In contrast, when too much PVP was dissolved (800 mg, eight times more than in the typical condition), only solid particles were obtained (Figure S7b). PVP molecules tend to adsorb on the nanoparticle surface very easily due to the binding of its amide unit to iron ions.[23] The PVP layers protecting the shells can decrease the etching rate on the particle surface.[22]

When H^+ ions diffused into the PB mesocrystals, the local concentration of H^+ ions in the center part of the PB mesocrystals was higher than that on the particle surface. The etching rate in the center became relatively high, thereby forming the interior hollow cavity.[22] Without the protection of PVP layers, the H^+ ions were uniformly distributed over the entire region of the PB mesocrystals. Thus, the etching reaction happened throughout the mesocrystals, leading to the random formation of macro/mesoporous structures, as shown in Figure S7a. Under much thicker PVP protection, H^+ ions were unable to diffuse at all. Therefore, the etching reaction did not proceed well, which corresponded to the fact that the average particle sizes did not change much after the etching process.

The FTIR spectra of both hollow and solid PB mesocrystals are shown in Figure S8. Very similar spectra are visible, both presenting a stretching band at 2084 cm^{-1} originating from the typical C≡N bond of the PB crystal.[24] The peaks at 499 cm^{-1}, which are associated with the Fe–C≡N–Fe bending modes,[24] are also observable. It should be noted that the positions of the peaks were not changed at all, even after the etching treatment. The Fe–C≡N–Fe bending modes are especially sensitive to interstitial alkali cations. Therefore, if alkali cations in the interstitial sites (for example, interstitial K^+) are introduced by the etching process, the peak positions must be shifted.[24] From the FTIR spectra, we can rule out the possibility of the introduction of alkali cations.

To explore potential applications, magnetic properties of the solid PB mesocrystal (as the starting material; Figure S1a) and the obtained hollow PB mesocrystal (Figure S1c) were investigated. Figure S9 shows field-cooled magnetization curves under an external magnetic field of 50 G. Both samples showed similar Curie temperatures (T_c) of around 5 K (Figure S9), corresponding to the previously reported results for bulk PB[25] and PB nanocubes with 90 nm in size.[26] The magnetic field dependence of the magnetization at 2.0 K (Figure 2a) clearly illustrated that both samples showed ferromagnetic properties rather than superparamagnetic behavior, even though the PB mesocrystals were constructed from small PB nanocrystals.

It is noteworthy that morphological differences between solids and hollows in the PB mesocrystals had a strong impact on the magnetization process. In both samples, the saturation magnetizations (M_s) were almost the same (around 66 emu g^{-1}) under an applied magnetic field of 1.0×10^3 Oe (Figure 2a). However, a large difference in the hysteresis shapes was confirmed. The remanent magnetization (M_r) of a hollow PB mesocrystal (21.3 emu g^{-1}) was much larger than that of a solid PB mesocrystal (7.0 emu g^{-1}). The atomic-scale magnetic interaction between Fe^{3+} sites through NC–Fe^{II}–CN linkages would not have influenced the magnetic property because the PB mesocrystals were assembled from the same small PB nanoparticles with an oriented attachment. Therefore, the enhancement of the M_r value of a hollow PB mesocrystal is most likely attributable to a change in shape-dependent magnetic anisotropy owing to the existence of the interior hollow cavity.

The difference in magnetization processes between solid and hollow PB mesocrystals can be reasonably explained by

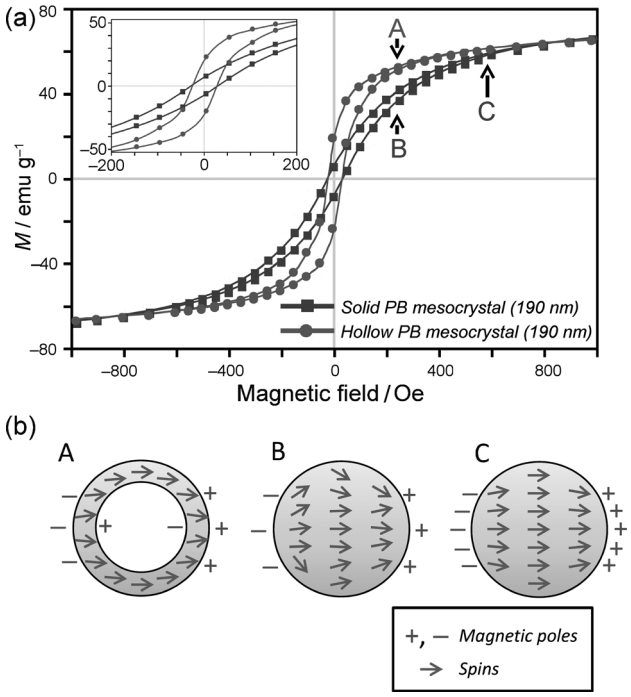

Figure 2. a) Field dependence of the magnetization at 2.0 K. Inset: expansion within ±200 Oe. b) Illustration of the magnetization process and magnetic poles under a field application. Hollow PB mesocrystal (spherical shell) is at position A in (a) and solid PB mesocrystal (sphere) is at B and C in (a). "+" and "−" indicate the formed magnetic poles that are due to the local spin alignment in the mesocrystals.

an effective demagnetization factor ($N_{effective}$) as follows. We can assume that the shapes of the solid PB and hollow PB mesocrystals are a sphere and spherical shell, respectively (Figure 2b), because both samples are randomly dispersed in the direction of the applied magnetic field. We also assume that there was no exchange interaction between the mesocrystals. Based on these assumptions, the $N_{effective}$ of the solid PB mesocrystal is about 1/3 (demagnetization factor for a sphere), indicating a significant effect of the magnetic poles on the surface of the solid PB mesocrystals (Figure 2b, B and C). Under the magnetic field which can almost saturate the hollow PB mesocrystals (Position A in Figure 2a), local magnetic moments (spins) in the solid mesocrystals are not completely aligned along a magnetic field, leading to the decrease in M_r and the squareness of the hysteresis (Figure 2b, B). In fact, we found a small value of M_r in the solid PB mesocrystals. In contrast, the hollow PB mesocrystals have no magnetic substance inside their sphere shells, which softened the effect of the magnetic poles. Thus, each hollow PB mesocrystal can be easily magnetized along the sphere shell, as shown in Figure 2b, A. Therefore, the $N_{effective}$ of the hollow PB mesocrystal must have been significantly smaller than that in the solid PB mesocrystal ($0 < N_{effective} < 1/3$). As a result, by creating the hollow cavity, both the M_r value and the squareness of the magnetization curve were enhanced without a coercive (H_c) change. This example demonstrates that magnetic hysteresis can be designed by morphological control.

In conclusion, we developed a facile way to fabricate highly crystalline PB hollow particles with uniform sizes via a controlled self-etching reaction on PB mesocrystals. This method is widely applicable to other PB analogues and various kinds of mesocrystals, such as biominerals, semiconductors, coordination polymers, and organic dyes.[27] Our PB hollow particles possessed a hierarchical pore system, thus showing great potential for applications in catalytic and biomedical fields. One potential application is as a drug carrier, as the micropores can be used to adsorb small molecules and the mesopores allow large molecules (or particles) to access the macrosized cavity. Another potential application is magnetic separation of paramagnetic molecules from diamagnetic molecules.[28] The PBs, which are well-known as molecular magnets, are expected to serve as microporous magnets with significant magnetization hysteresis. By using our hollow PB particles, large hollow space can further increase loading capability of guest molecules. It is of great interest to explore new magnetic property of such hollow PB nanoparticles.

Experimental Section

(Poly(vinylpyrrolidone) (PVP, K30) and aq. HCl were obtained from Nacalai Tesque. $K_3[Fe(CN)_6]\cdot 3H_2O$ was purchased from Wako Pure Chemical Industries, Ltd.

110 nm mesocrystals: In a typical procedure, PVP (3 g) and $K_3[Fe(CN)_6]\cdot 3H_2O$ (131.7 mg) were added to HCl solution (0.01 M, 40 mL) under magnetic stirring. After 30 min of stirring, a clear solution was obtained. The vial was the placed into an electric oven and heated at 80 °C for 20 h. After aging, the precipitates were collected by centrifugation and washed in distilled water and ethanol several times. After drying at room temperature for 12 h, PB mesocrystals (110 nm), hereafter called solid PB mesocrystals (110 nm), were obtained.

190 nm mesocrystals: In a typical procedure, PVP (3 g) and $K_3[Fe(CN)_6]\cdot 3H_2O$ (131.7 mg) were added to HCl solution (0.1 M, 40 mL) under magnetic stirring. After 30 min of stirring, clear solution was obtained. Then, the vial was placed into an electric oven and heated at 80 °C for 20 h. After the aging, the precipitates were collected by centrifugation and washed in distilled water and ethanol several times. After drying at room temperature for 12 h, the resulting powder was obtained and used as seed for the next step. The seed (10 mg), PVP (3.0 g), and $K_3[Fe(CN)_6]\cdot 3H_2O$ (131.7 mg) were then added to HCl solution (0.01 M, 40 mL) under magnetic stirring. After 30 min of stirring, a clear solution was obtained. The vial was then placed into an electric oven and heated at 80 °C for 20 h. After aging, the precipitates were collected by centrifugation and washed in distilled water and ethanol several times. After drying at room temperature for 12 h, the PB mesocrystals (190 nm), hereafter called solid PB mesocrystals (190 nm), were obtained.

Preparation of Prussian blue (PB) single crystals: In a typical procedure, $K_3[Fe(CN)_6]\cdot 3H_2O$ (168.9 mg) was added to HCl solution (0.1 M, 40 mL) under magnetic stirring. After 5 min of stirring, a clear solution was obtained. The vial was the placed into an electric oven and heated at 80 °C for 20 h. After aging, the precipitates were collected by centrifugation and washed in distilled water and ethanol several times. After drying at room temperature for 12 h, PB single crystals were obtained.

Conversion of solid PB mesocrystals into hollow PB mesocrystals: In a typical procedure, solid PB mesocrystals (20 mg) and PVP (100 mg) were added to HCl solution (1.0 M, 20 mL) in a Teflon vessel under magnetic stirring. After 2 h, the vessel was transferred into a stainless autoclave and heated at 140 °C for 4 h in an electric oven. After aging, the precipitates were collected by centrifugation and washed in distilled water and ethanol several times. After drying at room temperature for 12 h, hollow PB mesocrystals were obtained.

SEM images were taken with a Hitachi SU-8000 scanning microscope at an accelerating voltage of 5 kV. TEM observation was performed using a JEM-2010 TEM system operated at 200 kV. Wide-angle powder X-ray diffraction (XRD) patterns were obtained with a Rigaku RINT 2500X diffractometer using monochromated $Cu_{K\alpha}$ radiation (40 kV, 40 mA) at a scanning rate of $0.5° min^{-1}$. Nitrogen adsorption–desorption isotherms were obtained by using a Quantachrome Autosorb Automated Gas Sorption System at 77 K. Magnetic susceptibilities of all the samples were measured with Quantum Design MPMS-XL5R SQUID. FTIR spectra were obtained using a Nicolet Nexus 670 FTIR spectrometer.

Received: July 24, 2011
Revised: October 27, 2011
Published online: December 16, 2011

Keywords: coordination polymers · hollow structures · mesoporous materials · Prussian blue

[1] a) X. W. Lou, L. A. Archer, Z. Yang, *Adv. Mater.* **2008**, *20*, 3987 – 4019; b) Y. Ma, L. Qi, *J. Colloid Interface Sci.* **2009**, *335*, 1 – 10.

[2] a) X. W. Lou, Y. Wang, C. Yuan, J. Y. Lee, L. A. Archer, *Adv. Mater.* **2006**, *18*, 2325 – 2329; b) X. W. Lou, C. M. Li, L. A. Archer, *Adv. Mater.* **2009**, *21*, 2536 – 2539; c) J. Liu, H. Xia, D. Xue, L. Lu, *J. Am. Chem. Soc.* **2009**, *131*, 12086 – 12087.

[3] a) J. Yu, H. Yu, H. Guo, M. Li, S. Mann, *Small* **2008**, *4*, 87 – 91; b) F. Cheng, H. Ma, Y. Li, J. Chen, *Inorg. Chem.* **2007**, *46*, 788 – 794.

[4] a) S. E. Skrabalak, J. Chen, Y. Sun, X. Lu, L. Au, C. M. Cobley, Y. Xia, *Acc. Chem. Res.* **2008**, *41*, 1587 – 1595; b) J. Chen, M. Yang, Q. Zhang, E. C. Cho, C. M. Cobley, C. Kim, C. Glaus, L. V. Wang, M. J. Welch, Y. Xia, *Adv. Funct. Mater.* **2010**, *20*, 3684 – 3694.

[5] a) Y. Piao, J. Kim, H. B. Na, D. Kim, J. S. Baek, M. K. Ko, J. H. Lee, M. Shokouhimehr, T. Hyeon, *Nat. Mater.* **2008**, *7*, 242 – 247; b) S. Tang, X. Huang, X. Chen, N. Zheng, *Adv. Funct. Mater.* **2010**, *20*, 2442 – 2447.

[6] a) F. Caruso, R. A. Caruso, H. Möhwald, *Science* **1998**, *282*, 1111 – 1114; b) M. S. Wong, J. N. Cha, K. S. Choi, T. J. Deming, G. D. Stucky, *Nano Lett.* **2002**, *2*, 583 – 587; c) Y. Sun, Y. Xia, *Science* **2002**, *298*, 2176 – 2179; d) D. H. Son, S. M. Hughes, Y. Yin, A. P. Alivisatos, *Science* **2004**, *306*, 1009 – 1012; e) B. Liu, H. C. Zeng, *Small* **2005**, *1*, 566 – 571; f) H. Xu, W. Wang, *Angew. Chem.* **2007**, *119*, 1511 – 1514; *Angew. Chem. Int. Ed.* **2007**, *46*, 1489 – 1492; g) T. Zhang, J. Ge, Y. Hu, Q. Zhang, S. Aloni, Y. Yin, *Angew. Chem.* **2008**, *120*, 5890 – 5895; *Angew. Chem. Int. Ed.* **2008**, *47*, 5806 – 5811; h) C. H. Kuo, M. H. Huang, *J. Am. Chem. Soc.* **2008**, *130*, 12815 – 12820; i) R. Levi, M. Bar-Sadan, A. Albu-Yaron, R. Popovitz-Biro, L. Houben, C. Shahar, A. Enyashin, G. Seifert, Y. Prior, R. Tenne, *J. Am. Chem. Soc.* **2010**, *132*, 11214 – 11222; j) D. Aherne, M. Gara, J. M. Kelly, Y. K. Gun′ko, *Adv. Funct. Mater.* **2010**, *20*, 1329 – 1338.

[7] a) F. Caruso, *Chem. Eur. J.* **2000**, *6*, 413 – 419; b) C. S. Peyratout, L. Dähne, *Angew. Chem.* **2004**, *116*, 3850 – 3872; *Angew. Chem. Int. Ed.* **2004**, *43*, 3762 – 3783; c) X. Shi, M. Shen, H. Möhwald, *Prog. Polym. Sci.* **2004**, *29*, 987 – 1019.

[8] a) X. W. Lou, D. Deng, J. Y. Lee, L. A. Archer, *Chem. Mater.* **2008**, *20*, 6562 – 6566; b) T. He, D. Chen, X. Jiao, Y. Xu, Y. Gu, *Langmuir* **2004**, *20*, 8404 – 8408; c) X. W. Lou, L. A. Archer, *Adv. Mater.* **2008**, *20*, 1853 – 1858.

[9] a) F. Gyger, M. Hübner, C. Feldmann, N. Barsan, U. Weimar, *Chem. Mater.* **2010**, *22*, 4821 – 4827; b) H. Zhang, Q. Zhu, Y.

Zhang, Y. Wang, L. Zhao, B. Yu, *Adv. Funct. Mater.* **2007**, *17*, 2766 – 2771.
[10] L. Jin, L. Xu, C. Morein, C. Chen, M. Lai, S. Dharmarathna, A. Dobley, S. L. Suib, *Adv. Funct. Mater.* **2010**, *20*, 3373 – 3382.
[11] a) Y. Zhu, J. Shi, W. Shen, X. Dong, J. Feng, M. Ruan, Y. Li, *Angew. Chem.* **2005**, *117*, 5213 – 5217; *Angew. Chem. Int. Ed.* **2005**, *44*, 5083 – 5087; b) L. Zhang, S. Qiao, Y. Jin, Z. Chen, H. Gu, G. Q. Lu, *Adv. Mater.* **2008**, *20*, 805 – 809.
[12] a) O. M. Yaghi, M. O'Keeffe, N. W. Ockwig, H. K. Chae, M. Eddaoudi, J. Kim, *Nature* **2003**, *423*, 705 – 714; b) X. Zhao, B. Xiao, A. J. Fletcher, K. M. Thomas, D. Bradshaw, M. J. Rosseinsky, *Science* **2004**, *306*, 1012 – 1015; c) S. Horike, S. Shimomura, S. Kitagawa, *Nat. Chem.* **2009**, *1*, 695 – 704; d) S. T. Meek, J. A. Greathouse, M. D. Allendorf, *Adv. Mater.* **2011**, *23*, 249 – 267; e) M. I. H. Mohideen, B. Xiao, P. S. Wheatley, A. C. McKinlay, Y. Li, A. M. Z. Slawin, D. W. Aldous, N. F. Cessford, T. Düren, X. Zhao, R. Gill, K. M. Thomas, J. M. Griffin, S. E. Ashbrook, R. E. Morris, *Nat. Chem.* **2011**, *3*, 304 – 310; f) A. C. McKinlay, R. E. Morris, P. Horcajada, G. Férey, R. Gref, P. Couvreur, C. Serre, *Angew. Chem.* **2010**, *122*, 6400 – 6406; *Angew. Chem. Int. Ed.* **2010**, *49*, 6260 – 6266.
[13] a) M. E. Davis, *Nature* **2002**, *417*, 813 – 821; b) M. E. Kosal, J. H. Chou, S. R. Wilson, K. S. Suslick, *Nat. Mater.* **2002**, *1*, 118 – 121; c) Y. Fang, H. Hu, G. Chen, *Chem. Mater.* **2008**, *20*, 1670 – 1672.
[14] a) X. D. Wang, W. L. Yang, Y. Tang, Y. J. Wang, S. K. Fub, Z. Gao, *Chem. Commun.* **2000**, 2161 – 2162; b) A. Dong, N. Ren, W. Yang, Y. Wang, Y. Zhang, D. Wang, J. Hu, Z. Gao, Y. Tang, *Adv. Funct. Mater.* **2003**, *13*, 943 – 948; c) N. Chu, J. Wang, Y. Zhang, J. Yang, J. Lu, D. Yin, *Chem. Mater.* **2010**, *22*, 2757 – 2763; d) R. Ameloot, F. Vermoortele, W. Vanhove, M. B. J. Roeffaers, B. F. Sels, D. E. De Vos, *Nat. Chem.* **2011**, *3*, 382 – 387; e) G. Liang, J. Xu, X. Wang, *J. Am. Chem. Soc.* **2009**, *131*, 5378 – 5379; f) R. McHale, N. Ghasdian, Y. Liu, M. B. Ward, N. S. Hondow, H. Wang, Y. Miao, R. Brydson, X. Wang, *Chem. Commun.* **2010**, *46*, 4574 – 4576; g) X. Roy, J. K. H. Hui, M. Rabnawaz, G. Liu, M. J. MacLachlan, *J. Am. Chem. Soc.* **2011**, *133*, 8420 – 8423.
[15] J. Huo, L. Wang, E. Irran, H. Yu, J. Gao, D. Fan, B. Li, J. Wang, W. Ding, A. M. Amin, C. Li, L. Ma, *Angew. Chem.* **2010**, *122*, 9423 – 9427; *Angew. Chem. Int. Ed.* **2010**, *49*, 9237 – 9241.
[16] a) N. R. de Tacconi, K. Rajeshwar, R. O. Lezna, *Chem. Mater.* **2003**, *15*, 3046 – 3062; b) S. Ohkoshi, K. Arai, Y. Sato, K. Hashimoto, *Nat. Mater.* **2004**, *3*, 857 – 861; c) Z. Chu, Y. Zhang, X. Dong, W. Jin, N. Xu, B. Tieke, *J. Mater. Chem.* **2010**, *20*, 7815 – 7820; d) S. Ferlay, T. Mallah, R. Quahès, P. Veillet, M. Verdaguer, *Nature* **1995**, *378*, 701 – 703; e) P. Dechambenoit, J. R. Long, *Chem. Soc. Rev.* **2011**, *40*, 3249 – 3265; f) M. Shokouhimehr, E. S. Soehnlen, J. Hao, M. Griswold, C. Flask, X. Fan, J. P. Basilion, S. Basu, S. D. Huang, *J. Mater. Chem.* **2010**, *20*, 5251 – 5259.
[17] a) H. Cölfen, M. Antonietti, *Angew. Chem.* **2005**, *117*, 5714 – 5730; *Angew. Chem. Int. Ed.* **2005**, *44*, 5576 – 5591; b) H. Cölfen, S. Mann, *Angew. Chem.* **2003**, *115*, 2452 – 2468; *Angew. Chem. Int. Ed.* **2003**, *42*, 2350 – 2365.
[18] a) M. Hu, J. S. Jiang, R. P. Ji, Y. Zeng, *CrystEngComm* **2009**, *11*, 2257 – 2259; b) M. Hu, J. S. Jiang, C. C. Lin, Y. Zeng, *CrystEngComm* **2010**, *12*, 2679 – 2683.
[19] a) S. S. Kaye, J. R. Long, *J. Am. Chem. Soc.* **2005**, *127*, 6506 – 6507; b) S. S. Kaye, J. R. Long, *Catal. Today* **2007**, *120*, 311 – 316.
[20] M. Hu, J. S. Jiang, Y. Zeng, *Chem. Commun.* **2010**, *46*, 1133 – 1135.
[21] a) C. M. Cobley, M. Rycenga, F. Zhou, Z. Y. Li, Y. Xia, *Angew. Chem.* **2009**, *121*, 4918 – 4921; *Angew. Chem. Int. Ed.* **2009**, *48*, 4824 – 4827; b) T. Soejima, N. Kimizuka, *J. Am. Chem. Soc.* **2009**, *131*, 14407 – 14412; c) M. J. Mulvihill, X. Y. Ling, J. Henzie, P. Yang, *J. Am. Chem. Soc.* **2010**, *132*, 268 – 274.
[22] Q. Zhang, T. Zhang, J. Ge, Y. Yin, *Nano Lett.* **2008**, *8*, 2867 – 2871.
[23] a) T. Uemura, S. Kitagawa, *J. Am. Chem. Soc.* **2003**, *125*, 7814 – 7815; b) Z. Li, J. Zhang, T. Mu, J. Du, Z. Liu, B. Han, J. Chen, *Colloids Surf. A* **2004**, *243*, 63 – 66.
[24] R. E. Wilde, S. N. Ghosh, B. J. Marshall, *Inorg. Chem.* **1970**, *9*, 2512 – 2516.
[25] T. Uemura, M. Ohba, S. Kitagawa, *Inorg. Chem.* **2004**, *43*, 7339 – 7345.
[26] Y. Ding, Y. L. Hu, G. Gu, X. H. Xia, *J. Phys. Chem. C* **2009**, *113*, 14838 – 14843.
[27] a) M. Kijima, Y. Oaki, H. Imai, *Chem. Eur. J.* **2011**, *17*, 2828 – 2832; b) Y. Oaki, H. Imai, *Bull. Chem. Soc. Jpn.* **2009**, *82*, 613 – 617; c) H. Imai, Y. Oaki, A. Kotachi, *Bull. Chem. Soc. Jpn.* **2006**, *79*, 1834 – 1851; d) R. Q. Song, H. Cölfen, *Adv. Mater.* **2010**, *22*, 1301 – 1330.
[28] L. G. Beauvais, J. R. Long, *J. Am. Chem. Soc.* **2002**, *124*, 12096 – 12097.

